

Article

Surface Subsidence Prediction Method for Backfill Mining in Shallow Coal Seams with Hard Roofs for Building Protection

Wenqi Huo ^{1,2}, Huaizhan Li ^{1,2,*} , Guangli Guo ^{1,2}, Yuezong Wang ^{1,2} and Yafei Yuan ²

¹ Key Laboratory of Resources and Environment Information Engineering, China University of Mining and Technology, Xuzhou 221116, China; huowenqi@cumt.edu.cn (W.H.); guo_gl123@163.com (G.G.); 19154508130@163.com (Y.W.)

² School of Environment Science and Spatial Informatics, China University of Mining and Technology, Xuzhou 221116, China; yuanyafei@cumt.edu.cn

* Correspondence: lihuaizhan@cumt.edu.cn; Tel.: +86-136-1510-4142

Abstract: The mining of shallow coal seams with hard roofs poses a threat to surface structures. In order to ensure the protection of these buildings, backfill mining is increasingly used in these types of coal seams. However, due to the lack of appropriate surface subsidence prediction methods, there are concerns about whether backfill mining can meet the requirements of building protection. In this study, through numerical simulation and physical experiments, the movement characteristics of the strata and surface were studied in the backfill mining of a shallow coal seam with a hard roof. Our results indicate that the backfilling ratio significantly influences strata movement and surface subsidence. As the backfilling ratio increases, the surface deformation in the backfill under the hard roof of the shallow coal seam transitions from discontinuous to continuous. When the backfilling ratio exceeds 60%, the deformation characteristics of the overburden and surface align with the probability integral method model. Consequently, a novel surface subsidence prediction method for backfill mining in shallow coal seams under hard roofs is proposed. This method was successfully applied at Yungang Mine, validating its effectiveness. These research findings have significant practical implications for the design of backfill mining in shallow coal seams under hard roofs.

Keywords: numerical simulation; backfill mining; shallow coal seam mining under hard roof; subsidence prediction



Citation: Huo, W.; Li, H.; Guo, G.; Wang, Y.; Yuan, Y. Surface Subsidence Prediction Method for Backfill Mining in Shallow Coal Seams with Hard Roofs for Building Protection. *Sustainability* **2023**, *15*, 15791. <https://doi.org/10.3390/su152215791>

Academic Editors: Fei Tan, Qiao Wang, Huachuan Wang and Defu Tong

Received: 9 October 2023
Revised: 1 November 2023
Accepted: 2 November 2023
Published: 9 November 2023



Copyright: © 2023 by the authors. Licensee MDPI, Basel, Switzerland. This article is an open access article distributed under the terms and conditions of the Creative Commons Attribution (CC BY) license (<https://creativecommons.org/licenses/by/4.0/>).

1. Introduction

Coal plays a significant role in global primary energy consumption. However, while coal mining brings substantial economic benefits, it also contributes to environmental degradation. Once the coal is extracted, the overlying rock strata undergo movement and deformation, transferring these effects upward towards the surface. This process leads to surface subsidence, which can cause damage to buildings and structures. Therefore, the accurate prediction of surface subsidence is crucial for implementing measures that protect these structures [1–4]. By predicting surface movement and deformation, the appropriate mining method is selected to reduce damage to buildings [5–8]. Zhang et al. analyzed the influence of the bulk ratio of waste and fly ash backfilling material on the movement of the overlying strata and surface subsidence control in backfill mining. Their study determined an optimal bulk ratio of backfilling material that ensures a reasonable range of surface subsidence [9]. In a separate study, Guo et al. proposed theories and methods for coordinated subsidence control in green mining, with a particular emphasis on protecting cultivated land [10].

For the majority of surface subsidence brought on by underground mining, the conventional technique of surface subsidence prediction is appropriate [11–17]. However, it is difficult for the hard roof created during shallow coal seam mining to naturally collapse after mining, leaving a sizable part of the goaf with a hanging roof. When the hanging

roof area reaches a critical point, the accumulated energy within the roof and coal seam is suddenly released, leading to an abrupt roof rupture. This phenomenon can trigger dynamic mine disasters such as rock bursts and large-scale weighting [18,19]. To prevent such disasters, the method of forced caving is commonly employed [20,21]. However, this approach often results in surface collapse pits and other forms of discontinuous damage. Due to these unique characteristics, surface subsidence in this scenario does not conform to the traditional mining subsidence theory. As a result, the conventional mining subsidence prediction methods are inadequate for accurately predicting surface subsidence.

A large number of studies and engineering practices have proved that backfill mining can effectively control surface subsidence and solve the dynamic problem of mining under a hard roof. Using the goaf filling ratio (the difference between mining thickness and equivalent mining height is divided by mining thickness), the surface movement and deformation can be controlled within the allowable damage range of buildings [22–29]. Scholars have conducted research on the backfill mining of shallow coal seams. Bai et al. [30] suggested that the utilization of aeolian sand-based backfill material in shallow and thick underground coal seam mining can effectively protect the eco-environment and control geo-environmental hazards. Liu et al. [31] proposed a structured backfill mining method incorporating high-water materials and pillars, along with a surface subsidence prediction model. Sun et al. [32] suggested three backfill mining methods to address major geo-environmental hazards caused by shallow coal mining in eco-environmentally fragile areas of western China. While there have been several studies on backfill mining, they primarily focus on general geological conditions, with limited research specifically addressing the backfill mining of shallow coal seams under hard roofs. The movement and deformation characteristics of the strata and surface after backfill mining remain unclear, and the prediction methods for surface subsidence are not well defined. Numerical and physical simulation methods are widely employed in this field [33–36]. Wesolowski, M et al. utilized computer simulation to examine the influence of mine working flooding on the surface of a mining area [37]. Rajwa, S et al. conducted numerical simulations to investigate the causes of damage to a longwall located beneath an unmined longwall panel [38]. These scholars obtained promising experimental results through simulation techniques.

Therefore, this paper focuses on the characteristics of strata movement and surface deformation due to backfill mining in a hard-roofed shallow coal seam of Yungang Coal Mine in Shanxi Province. This research adopts the methods of numerical simulation and theoretical analysis. In addition, a surface subsidence prediction method for backfill mining is proposed, and subsidence prediction is carried out for the Yungang Mine. The research results have important practical significance for the design and implementation of backfill mining in shallow coal seams with hard roofs.

2. Simulation Experiment

2.1. Overview of Study Area

The Yungang Minefield is situated in Datong City, Shanxi Province, China, and is owned by the Datong Coal Mine Group Liability Company. It is located in the northeastern corner of the Datong Coalfield, approximately 18 km away from Datong City. The administrative division of the mine falls under the jurisdiction of the southern suburb of Datong City.

The simulation study area focuses on mining the No. 3 coal seam. The average thickness of the No. 3 coal seam, based on drilling data in the study area, is 2 m. The average mining depth is 100 m, and the coal seam has a dip angle of 3° , which can be considered nearly horizontal. The No. 3 coal seam is located in the Datong Formation of the Middle Jurassic, which has a thickness of 176 m. It primarily consists of gray and gray-brown mudstone, as well as gray and gray-white sandstone, along with the coal seam. The stratum above the Datong Formation is the Yungang Formation, which has a thickness of 104 m and is composed of gray silty sandstone, gray sandstone, and conglomerate

rock. Above this stratum is the Quaternary, and the stratum in this section is thin, with a thickness of only 4 m. More detailed information on the strata can be found in Section 3.1.

The CT3401 working face is the first backfill mining face of the No. 3 coal seam. The working face measures 200 m in length and 150 m in width. The average thickness of the coal seam is 2 m, with a coal reserve of 79,000 tons for the working face. The overlying roof of the working face is composed of thick fine-grained sandstone, with an average thickness of about 20 m, and is dense and hard. The floor is composed of sandy mudstone and siltstone.

2.2. Numerical Model and Simulation Scheme

In order to accurately analyze the surface movement and deformation characteristics of backfill mining with different filling rates in the presence of a hard roof and a shallow, low coal seam, a comprehensive numerical model of the whole stratum was established using FLAC3D 5.0 numerical simulation software. The model is based on drilling data of the CT3401 working face in Yungang Mine. The size of the model is 600 m × 550 m × 110 m, the length and width of each unit are fixed to 10 m, and the height varies according to the strata. The model is divided into 36,300 units. The left and right boundaries of the model are fixed in the x direction, the front and rear boundaries are fixed in the y direction, the lower boundary is fixed in the z direction, and the top is free. The numerical model is shown in Figure 1. Because the Mohr–Coulomb criterion is widely used in rock mechanics, mining engineering, and other fields, this paper uses the Mohr–Coulomb criterion to study the characteristics of rock movement [39–41].

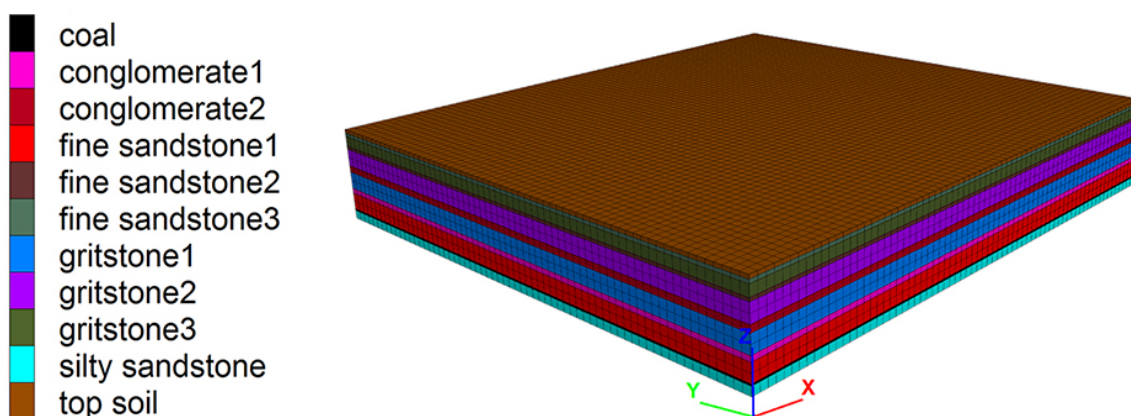


Figure 1. Numerical model of backfill mining in the CT3401 working face.

First, the model was calibrated. By referring to mining areas with similar geological conditions in the vicinity of the study area, the mechanical parameters of the model were assigned based on the rock stratum's mechanical characteristics. The excavation of the coal seam was simulated, and surface subsidence data under sufficient mining conditions were extracted. The subsidence coefficient was then calculated using Equation (1) and compared with the empirical subsidence coefficient of the mining area. When the two values were similar, the mechanical parameters for the rock simulation were determined. When the difference between the two values was large, the mechanical parameters of the simulation were adjusted until the subsidence coefficients obtained by the two were similar. As shown in Figure 2, the maximum subsidence value of the surface was about 1200 mm, the mining thickness of the research working face was 2 m, and the inclination angle of the coal seam was 3°, which can be regarded as horizontal. The simulated subsidence coefficient is 0.6, which aligns well with the empirical subsidence coefficient range of 0.5 to 0.65 for the Datong mining area [42,43]. This agreement indicates a good match between

the two values. Finally, the distribution of each rock layer and the simulated mechanical parameters of the mining area were determined.

$$q = \frac{W_0}{m \cdot \cos \alpha} \quad (1)$$

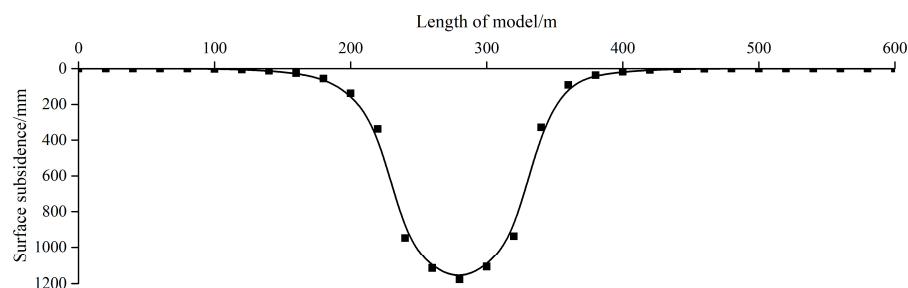


Figure 2. Surface subsidence curve of a fully mined coal seam.

In the above equation, W_0 is the maximum surface subsidence value; m is the mining thickness of the coal seam; and α is the dip angle of the coal seam.

The CT3401 working face was mined using gangue filling. The strike length of the working face was 200 m, and the dip length was 150 m. In the model, the corresponding units for backfill mining are within the range of 200–400 m in the strike direction and 200–350 m in the dip direction. The constitutive model used for each element in FLAC3D is Mohr–Coulomb. The distribution and simulated mechanical parameters of each stratum in the mining area are presented in Table 1.

Table 1. Simulated mechanical parameters of the mining area.

Rock Stratum	Thickness (m)	Bulk Modulus (GPa)	Shear Modulus (GPa)	Cohesion (MPa)	Tensile Strength (MPa)	Internal Friction Angle Φ ($^\circ$)	Density (kg/m^3)
Top soil	4	0.25	0.16	0.10	0.05	15	1200
Fine sandstone	4	1.37	0.94	0.90	0.75	30	2400
Gritstone	12	1.07	0.74	0.80	0.65	30	2300
Fine sandstone	4	1.37	0.94	0.90	0.75	30	2400
Gritstone	20	0.96	0.61	0.70	0.60	30	2300
Conglomerate	8	1.15	0.73	0.80	0.70	28	2100
Gritstone	20	0.96	0.61	0.70	0.60	30	2300
Conglomerate	6	1.03	0.65	0.75	0.60	28	2100
Fine sandstone	20	1.56	1.16	1.20	0.90	35	2500
Coal	2	0.67	0.40	0.60	0.50	25	1800
Silty sandstone	10	5.00	4.00	4.00	3.50	35	2400

This model was used to simulate the fill mining and caving mining of the CT3401 working face with filling rates of 20%, 40%, 60%, and 80%, respectively. In the test, the stiffness of the filling body was changed by varying the elastic modulus of the filling body, and then, the filling rates of the filling body were adjusted. The filling rate parameters of the filling body are shown in Table 2. The parameter calibration method is consistent with the mechanical parameter calibration method for the rock stratum simulation. There was an advancement of 20 m from the open-cutting of the working face, which was repeated a total of 10 times. After the model was balanced at the end of each excavation, the data required for the analysis of overburden failure and surface movement and deformation were extracted from the model.

Table 2. The parameters of the filling ratio 20%, 40%, 60% and 80% of the backfill body.

Filling Ratio of the Backfill Body	Bulk Modulus (MPa)	Shear Modulus (MPa)	Cohesion (MPa)	Tensile Strength (MPa)	Internal Friction Angle Φ (°)	Density (kg/m ³)
Filling ratio of 20%	4	2	0.03	0.02	20	1000
Filling ratio of 40%	6.3	3.1	0.03	0.02	20	1000
Filling ratio of 60%	8.7	4.3	0.03	0.02	20	1000
Filling ratio of 80%	11.1	5.4	0.03	0.02	20	1000

2.3. Physical Simulation Experiment Design

The model dimensions are 3.0 m × 0.3 m × 1.1 m (length × width × height). The thickness of each stratum in the model was determined based on the scaled-down dimensions of the model and the simplified dimensions of the corresponding strata in the actual geological layers. To establish the material composition of each rock layer in the similar-material model, compression tests needed to be conducted on the model specimens to determine their mechanical properties. Initially, the mechanical parameters of each rock layer in the model were determined by considering the mechanical parameters of the corresponding layers in the actual geological formations and applying the dynamic similarity ratio between the prototype and the model. The mechanical properties of both the actual strata and the strata in the model are presented in Table 3.

Table 3. Mechanical properties of stratum prototype and model.

Rock Stratum	Actual Rock Properties			Model Rock Properties		
	Thickness (m)	Density (kg/m ³)	Single-Axis Compressive Strength (MPa)	Thickness (m)	Density (kg/m ³)	Single-Axis Compressive Strength (MPa)
Top soil	4	1200	5	4	1500	0.063
Fine sandstone	4	2400	110	4	1500	0.688
Gritstone	12	2300	70	12	1500	0.457
Fine sandstone	4	2400	110	4	1500	0.688
Gritstone	20	2200	70	20	1500	0.477
Conglomerate	8	2250	85	8	1500	0.567
Gritstone	20	2200	70	20	1500	0.477
Conglomerate	6	2250	85	6	1500	0.567
Fine sandstone	20	2400	130	20	1500	0.813
Coal	2	1600	30	2	1500	0.281
Silty sandstone	10	2500	100	10	1500	0.600

Based on the mechanical properties of each rock layer obtained in the model, a similar material was prepared according to a similar-material ratio table [44]. This similar material was then used to create a model test block using a mold. A compression experiment was conducted on the test block in the laboratory using a coal rock rheological testing machine. By comparing the obtained compressive strength value with the values in Table 2, the closest match determined the ratio of the corresponding rock layer. The final material matching results for each rock layer are presented in Table 4.

Table 4. Material ratio of each rock layer obtained by the similar-material model.

Rock Stratum	Ratio of Component/%			The Proportion of Each Component in the Cement/%		
	River sand	Mica Powder	Cement	Gypsum	Calcium Carbonate	
Top soil	80	17	3	50		50
Fine sandstone	73	15	12	50		50
Gritstone	74	16	10	70		30
Fine sandstone	73	15	12	50		50
Gritstone	74	16	10	70		30
Conglomerate	73	15	12	50		50
Gritstone	74	16	10	70		30
Conglomerate	73	15	12	50		50
Fine sandstone	71	13	16	70		30
Coal	79	16	5	70		30
Silty sandstone	71	13	16	70		30

3. Surface Subsidence Characteristics of Fill Mining in Shallow Coal Seam with a Hard Roof

3.1. Numerical Simulation Results and Analysis

(1) Surface subsidence characteristics of different filling ratio schemes in backfill mining

The surface subsidence values in the excavation area of the working face were extracted from the model. The relationship between the maximum surface subsidence value and the advancing distance of the working face for different filling ratio schemes in backfill mining is depicted in Figure 3. It can be observed that prior to the working face advancing to 140 m, the changes in maximum surface subsidence for different filling ratio schemes are continuous and gradual, with minimal differences in the maximum subsidence values. When the working face advances to 140 m, the difference between the maximum subsidence values of caving mining and backfill mining, with a filling ratio of 80%, is only 62 mm. However, as the advancing distance of the working face reaches 140 m to 160 m, the maximum subsidence value increases significantly for backfill mining, with filling ratios of 20% and 40%, as well as for caving mining. The lower the filling ratio, the greater the increase in the subsidence value. In the case of caving mining, the subsidence value increases by 973 mm, and the hard roof breaks. Conversely, for backfill mining with filling ratios of 60% and 80%, as the working face advances to 200 m, the subsidence value continues to change in a gradual and moderate manner without a sharp increase. This is attributed to the supportive role played by the filling material in maintaining the stability of the hard roof. Therefore, when the filling ratio in backfill mining exceeds 60%, the hard roof remains intact and stable, without breaking.

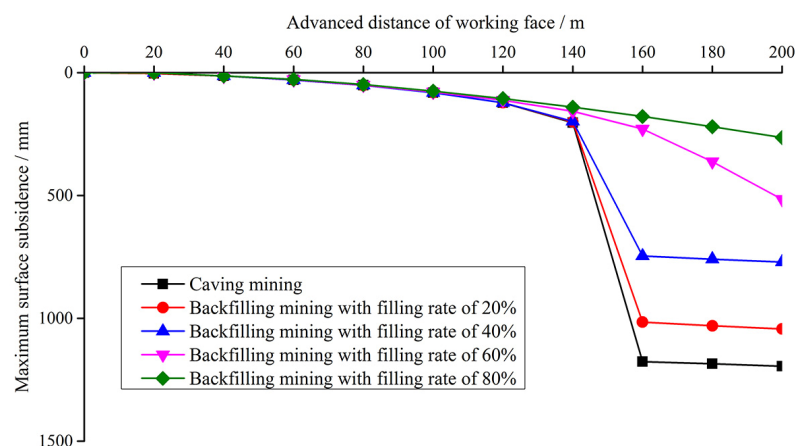


Figure 3. Relationship between maximum surface subsidence values and advancing distance of working face.

(2) Vertical stress distribution characteristics of different mining schemes along the main section

The proposed model can visually demonstrate the stress distribution within the rock layers. Figure 4 shows the vertical stress distribution of two different backfill mining schemes, with the caving mining and filling rates exceeding 60% in the main section of the CT3401 working face. The simulated mechanical parameters of these two schemes are shown in Table 5. It can be seen that after caving mining, the stress is mainly concentrated above the coal wall on both sides of the coal seam and in the center of the coal seam. The maximum longitudinal stress at the coal wall is about 6.4 MPa. The stress concentration in the center of the coal seam is caused by contact between the broken roof and the floor, resulting in the gradual compaction of the broken rock blocks. Additionally, an uncompacted area exists near the coal wall in the goaf, where the stress is about 70% and transfers towards the compacted area and the coal wall. In backfill mining with a 70% filling ratio, a vertical stress peak is only present on the coal wall, and the stress values are lower than those obtained for caving mining. The maximum vertical stress on the coal wall is reduced to 5 MPa, and the stress above the goaf is minimal. Conversely, in backfill mining with a 90% filling ratio, the overall stress distribution is more uniform. The stress on the coal wall is relatively higher than the internal stress of the filling material, at around 3.4 Mpa. Compared to the 70% filling ratio scheme, the stress on the coal wall is reduced, while the internal stress of the filling material increases, indicating that the filling material plays a more effective role in providing support.

Table 5. The parameters of the filling ratio 70% and 90% of the backfill body.

Filling Ratio of the Backfill Body	Bulk Modulus (MPa)	Shear Modulus (MPa)	Cohesion (MPa)	Tensile Strength (MPa)	Internal Friction Angle Φ (°)	Density (kg/m ³)
90% filling ratio	12.7	6.2	0.03	0.02	20	1000
70% filling ratio	9.5	4.7	0.03	0.02	20	1000

To further investigate the variation characteristics of vertical stress within the filling material in backfill mining and at the bottom plate in caving mining, the respective data were extracted and are presented in Figure 5. The vertical stress distribution in the caving mining method can be observed to exhibit three peaks, which are located within the coal wall and at the center of the goaf. Within the coal wall, a single stress peak is observed near 190 m and 400 m along the model's length, with a maximum stress value of approximately 6.2 MPa. On the other hand, the stress value at the center of the goaf in caving mining is smaller than that on the coal wall, reaching a maximum value of about 3.8 MPa. However, the range of stress variation is larger in this area. The original value of rock stress in the corresponding rock stratum is 2.15 MPa, while the stress value between 270 m and 330 m in the model exceeds 2.8 MPa. The stress variation trend in both backfill mining methods is consistent, featuring only a single peak on the coal wall. As the filling ratio increases, the stress on the coal wall decreases. For higher and lower filling ratios, the corresponding stress peaks are 4.5 MPa and 3.7 MPa, respectively. The stress distribution within the filling material is relatively uniform, but as the filling ratio increases, the stress inside the filling material also increases and gradually approaches the original value of rock stress. This can be attributed to the supportive effect of the filling material, which limits the sinking space of the roof. A higher filling ratio results in a larger contact area between the filling material and the roof, enhancing the bearing capacity. Consequently, the stress carried by the coal wall is continuously transferred to the filling material, bringing both stress levels closer to the original rock level.

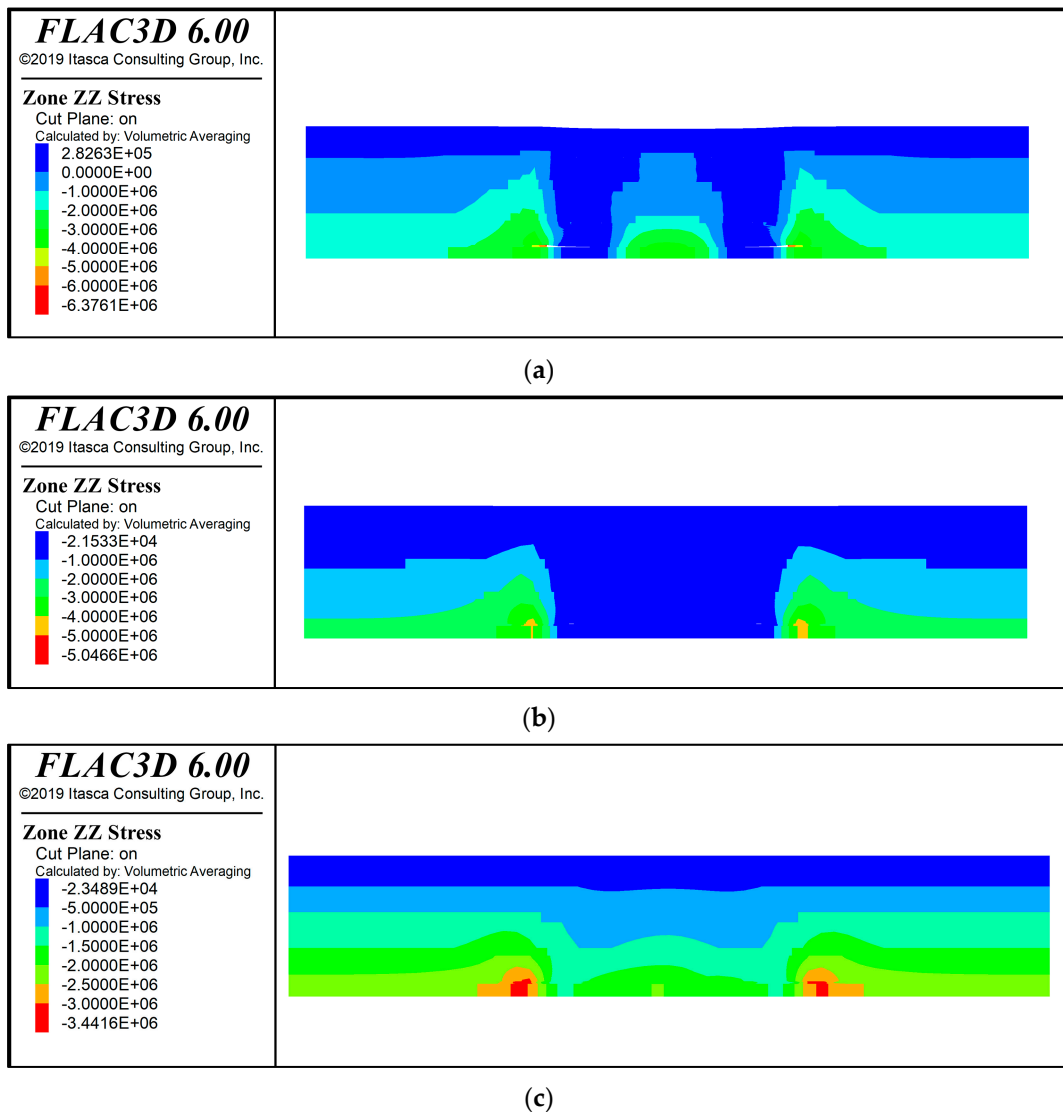


Figure 4. Vertical stress distribution of different mining schemes. (a) Vertical stress distribution of strata in caving mining. (b) Vertical stress distribution of strata in backfill mining with a 70% filling ratio. (c) Vertical stress distribution of strata in backfill mining with a 90% filling ratio.

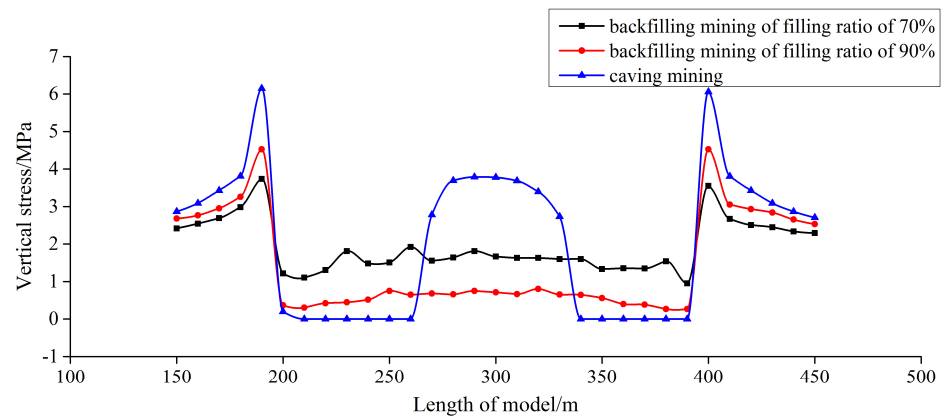


Figure 5. Vertical stress distribution of filling body along the strike direction in the main section.

(3) Surface movement and deformation law of different filling ratio schemes

After achieving stability in the ground movement basin, the distribution of movement and deformation in the main section typically follows certain patterns, including changes in subsidence, tilt, horizontal movement, horizontal deformation, and curvature. In Figure 5, surface movement and deformation curves are illustrated that correspond to filling ratios of 80% and 85% in backfill mining. It can be observed that the trends in subsidence, tilt, horizontal movement, and horizontal deformation are generally similar for both filling ratios, but their magnitudes differ. Specifically, as the filling ratio increases, the surface movement and deformation decrease.

Figure 6a depicts the surface subsidence curve, which exhibits symmetry with respect to the center of the basin. The maximum subsidence value is observed at the center of the basin, gradually decreasing from the center towards the edges until it reaches zero. On the other hand, Figure 6b,c illustrate the tilt curve and horizontal movement curve, respectively, both showing asymmetry around the center of the basin. These curves show an increasing trend from the edges of the basin towards the inflection point, reaching a maximum at the inflection point. From the inflection point to the maximum subsidence point, the values gradually decrease, eventually reaching zero at the point of maximum subsidence. In Figure 6d, the horizontal deformation curve exhibits symmetry with respect to the center of the basin. Positive values indicate the presence of a tensile zone, while negative values indicate compression. The curve shows four extrema: two positive extrema are observed between the boundary and the inflection point, while the other two negative extrema occur between the inflection point and the center of the goaf. Generally, the central part of the basin represents the compression zone, while the edges of the basin represent the tensile zone. At both the maximum subsidence point and the inflection point, the horizontal deformation reaches zero.

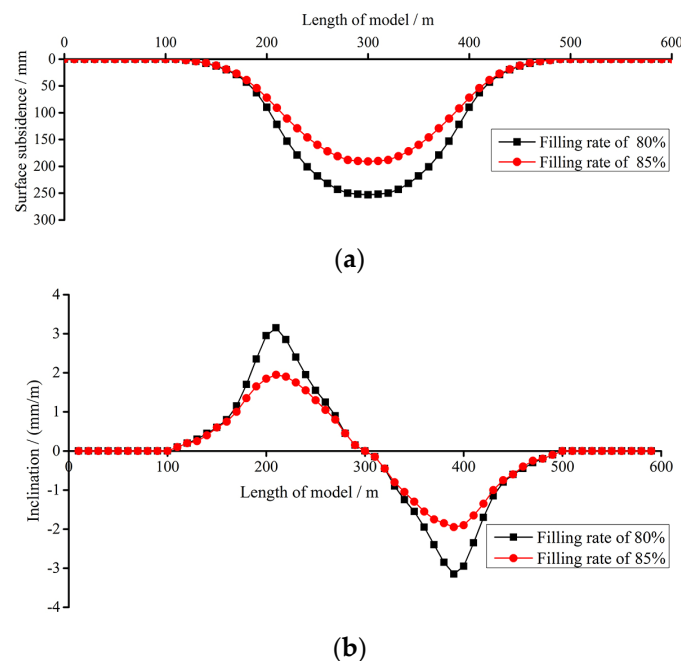


Figure 6. Cont.

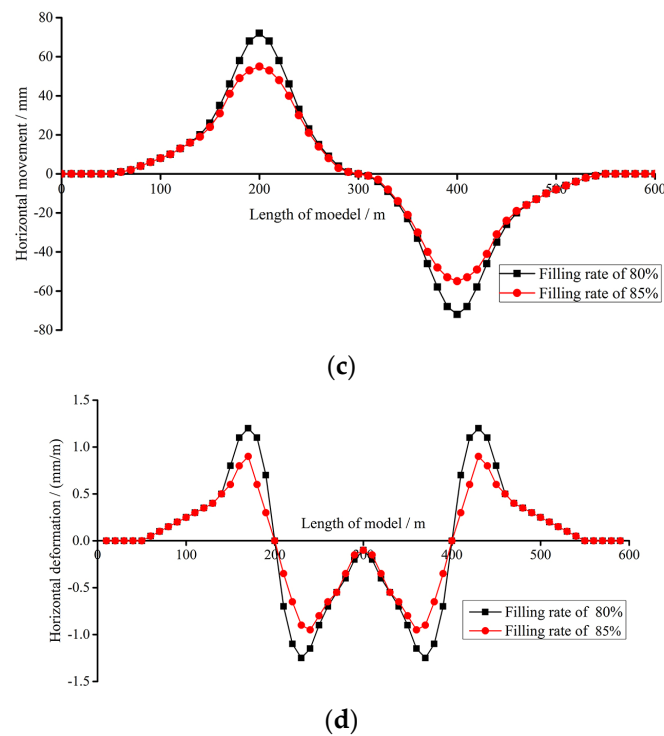


Figure 6. Surface movement and deformation curves for filling ratios of 80% and 85%. (a) Surface subsidence curve along the main section. (b) Tilt curve along the main section. (c) Horizontal movement curve along the main section. (d) Horizontal deformation curve along the main section.

Based on the above analysis, it can be concluded that mining a shallow coal seam under a hard roof with a high filling ratio exhibits overall variation characteristics that align closely with the surface movement and deformation patterns observed in the main section of a horizontally mined coal seam under full extraction. Moreover, the probability integral method prediction model proves accurate in forecasting these surface movement and deformation patterns.

3.2. Physical Simulation Results and Analysis

The overburden structure shows distinct zoning characteristics after mining. As shown in Figure 7, under typical geological and mining conditions, the overburden experiences stratum movement and stabilization, leading to the formation of three distinct zones of mining that are influenced by the degree of damage. These zones are commonly referred to, from bottom to top, as the caving zone, faulted zone, and bending zone. In backfill mining, once the compacted filling material achieves a certain level of strength, it provides support to the overlying roof, thereby reducing the available space for roof movement. The stress existing in the rock layer is partially transferred to the filling material, which helps to mitigate the impact of mining-induced stress on the mining process. As a result, the roof remains stable without collapsing, and only minor fractures or cracks may occur in the immediate roof. The primary type of deformation observed in the overlying strata is bending deformation. In this scenario, the overburden predominantly exhibits a well-defined layered structure and can be divided into two distinct zones along the normal direction of the layers: the fracture zone and the bending zone.

The characteristics of the overburden structure following mining in shallow coal seams with hard roofs differ from those under normal geological and mining conditions. Figure 8 represents a physical experiment conducted on caving mining and backfill mining in shallow coal seams.

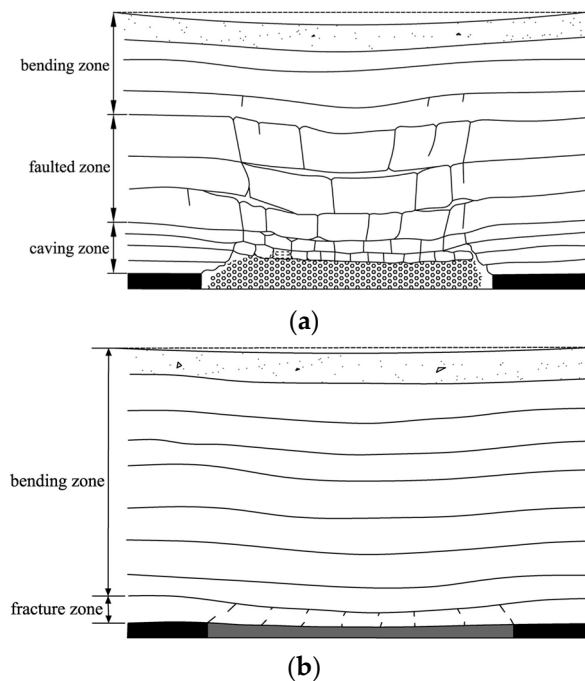


Figure 7. Schematic diagram of an overburden structure in deep coal mining. (a) Caving mining; (b) backfill mining.

Figure 8a shows the initial stage of caving mining, whereby the rock strata below the main key strata are fractured and collapsed. The main key strata are characterized by high strength and stiffness. While bending deformation occurs, the overlying strata also deform synchronously. As mining progresses, the strata under the primary key stratum continue to collapse, resulting in an increase in the exposed area and internal stress on the primary key stratum. Once the internal stress in the rock exceeds its tensile strength, the energy accumulated in the rock will be released rapidly. The destruction and instability of the main key stratum structure are revealed through the complete cutting of the full thickness on both sides of the coal wall, thus forming a large collapse pit on the surface. Based on the above analysis, it is clear that when the primary key stratum, such as a hard direct roof, is located directly above the coal seam in shallow coal seam mining, the initial stage of mining is characterized by bending deformation of the hard roof and synchronous deformation of the overburden. As the hard roof becomes unstable and fractures, the overlying rock experiences complete collapse. In comparison to general geological conditions in mining, the presence of a hard roof in shallow coal seam mining has a significant controlling effect on both the rock strata and the surface. The failure of the hard roof triggers the collapse of the overlying rock, resulting in severe surface subsidence. Consequently, the overburden structure is primarily composed of caving zones and faulted zones, without the existence of a bending zone.

Figure 8b–d show the process of hard roof backfill mining in shallow coal seams. With the progress of mining, the combined action of the filling materials and hard roof ensures that the stress inside the rock remains within the bearing capacity of the hard roof. Therefore, the roof undergoes bending deformation, and the development of rock cracks is limited. After mining is complete, the bending deformation of the roof reaches the maximum. The overall rock structure presents a complete layered structure, and the main type of deformation of the overlying rock is elastic bending. Compared with backfill mining under general geological conditions, there is no obvious fracture formation in the backfill mining of the shallow coal seam with a hard roof. On the contrary, the overlying rock mainly undergoes elastic bending deformation.

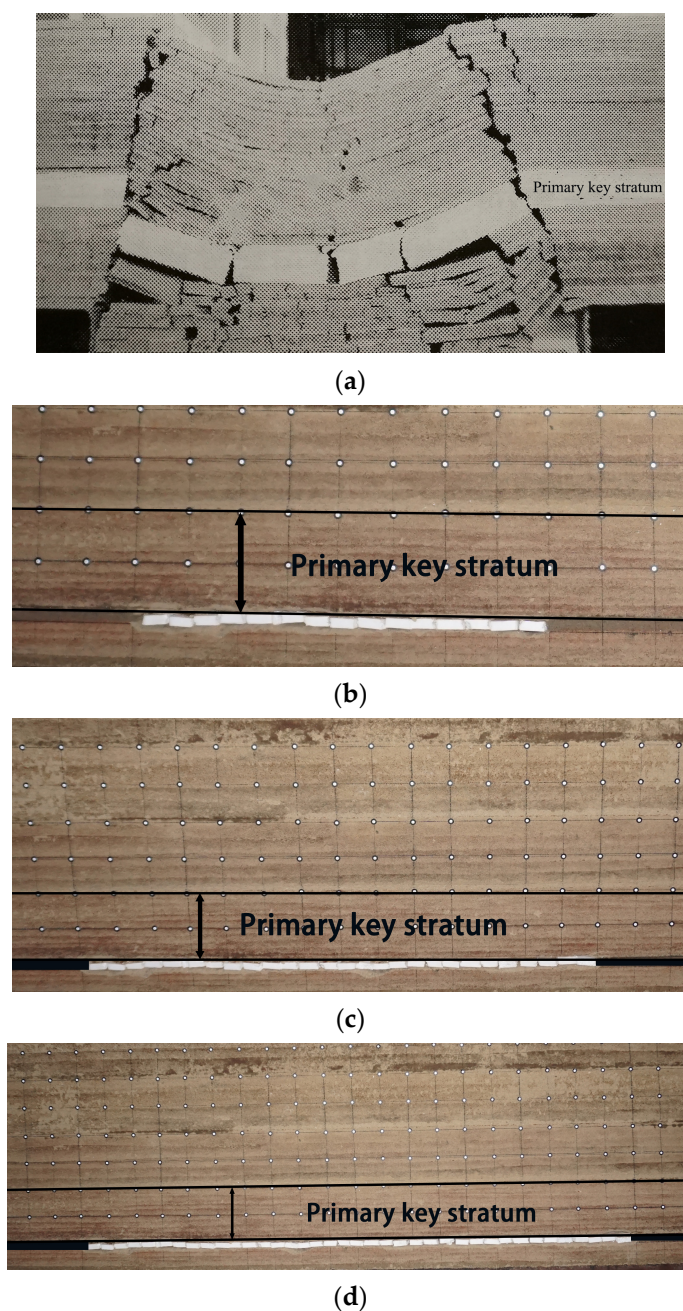


Figure 8. Similar-material models of shallow coal seam mining. (a) Caving mining [45]; (b) backfill mining (the advancing distance of the working face is 80 m); (c) backfill mining (the advancing distance of the working face is 140 m); (d) backfill mining (the advancing distance of the working face is 200 m).

4. Case Application

The CT3401 working face serves as the initial mining face for backfill mining. The area above the working face is densely populated with buildings, and coal extraction beneath these buildings is of significant concern. Surface subsidence resulting from mining operations in this working face can lead to damage to buildings and structures on the ground. Therefore, it is essential to predict surface subsidence prior to mining to enable the selection of an appropriate mining plan and the implementation of effective measures to safeguard the buildings and structures on the ground. The buildings and structures located above the CT3401 working face primarily consist of residential buildings, schools, high-voltage line towers, substations, and sewage treatment plants, among others. Based

on the characteristics of these buildings and structures, and with reference to relevant specifications [46], the protection criteria for the surface buildings and structures are as follows: the allowable inclined deformation value is 3.0 mm/m or less, the allowable horizontal deformation value is 2.0 mm/m or less, and the allowable curvature deformation value is 0.2 mm/m² or less.

4.1. Surface Subsidence Prediction Method

Based on the above analysis, it is concluded that the surface movement and deformation characteristics in the backfill mining of a shallow coal seam with a hard roof align with general mining principles. Extensive engineering practices and theoretical analyses support the prediction of these surface movement and deformation characteristics using the probability integral method. The mathematical model of the probability integral method can be expressed as follows:

The surface subsidence value at any point $A(x, y)$ is shown in Equation (2):

$$W(x, y)_A = W_0 C(x) C(y) \begin{cases} W_0 = mq \cos \alpha \\ C(x) = \frac{1}{\sqrt{\pi}} \left[\int_{-\sqrt{\pi} \frac{x}{r}}^0 e^{-\lambda^2} d\lambda + \int_0^{\sqrt{\pi} \frac{l-x}{r}} e^{-\lambda^2} d\lambda \right] \\ C(y) = \frac{1}{\sqrt{\pi}} \left[\int_{-\sqrt{\pi} \frac{y}{r_1}}^0 e^{-\lambda^2} d\lambda + \int_0^{\sqrt{\pi} \frac{L-y}{r_2}} e^{-\lambda^2} d\lambda \right] \end{cases} \quad (2)$$

where W_0 is the maximum surface subsidence value of full mining; m is the thickness of the coal seam; q is the surface subsidence coefficient; α is the dip angle of the coal seam; $C(x)$ and $C(y)$ are the subsidence distribution coefficients of point $A(x, y)$ in main strike and dip sections; l and L are the calculated mining widths along the strike and dip directions after considering the inflection point offset; r is the major influence radius of the strike direction; and r_1 and r_2 are the major influence radii of the dip direction, where r_1 is the downhill direction and r_2 is the uphill direction.

The tilt along the φ direction is shown in Equation (3):

$$i(x, y, \varphi) = i(x)C(y) \cos \varphi + i(y)C(x) \sin \varphi \quad (3)$$

where φ is the angle between the expected direction and the positive direction of the X axis (counter-clockwise rotation) and $i(x)$ and $i(y)$ are the tilt deformation values of point $A(x, y)$ in the main strike and dip sections under limited mining, respectively.

The curvature along the φ direction is shown in Equation (4):

$$K(x, y, \varphi) = K(x)C(y) \cos^2 \varphi + K(y)C(x) \sin^2 \varphi + \frac{i(x)i(y)}{W_0} \sin 2\varphi \quad (4)$$

where $K(x)$ and $K(y)$ are the curvature deformation values of point $A(x, y)$ in the main strike and dip sections under limited mining, respectively.

The horizontal movement along the φ direction is shown in Equation (5):

$$U(x, y, \varphi) = U(x)C(y) \cos \varphi + U(y)C(x) \sin \varphi \quad (5)$$

where $U(x)$ and $U(y)$ are the horizontal movement values of point $A(x, y)$ in the main strike and dip sections under limited mining, respectively.

The horizontal deformation along the φ direction is shown in Equation (6):

$$\varepsilon(x, y, \varphi) = \varepsilon(x)C(y) \cos^2 \varphi + \varepsilon(y)C(x) \sin^2 \varphi + \frac{U(x)U(y)}{W_0} \sin \varphi \cos \varphi \quad (6)$$

where $\varepsilon(x)$ and $\varepsilon(y)$ are the horizontal deformation values of point $A(x, y)$ in the main strike and dip sections under limited mining, respectively.

For backfill mining, the calculation of maximum surface subsidence in the ground movement basin is based on the principle of equivalent mining height. The theory of equivalent mining height refers to the difference between the actual mining height and the fully compacted thickness of the backfill material [47]. The calculated equivalent mining height is substituted with the actual mining height of the coal seam to obtain the maximum surface subsidence value. The calculation of equivalent mining height based on the filling ratio is shown in Equation (7):

$$m_d = m(1 - \rho) \quad (7)$$

where m_d is the equivalent mining height and ρ is the filling ratio of backfill mining.

4.2. Selection of Expected Parameters

Due to the limited availability of surface movement and deformation monitoring data for the Yungang coal mine, suitable parameters for predicting surface subsidence have not been established. Therefore, reference is made to the predicted parameters for surface movement and deformation in coal mines with similar geological conditions around the Yungang coal mine [42,43], as shown in Table 6.

Table 6. Prediction parameters of the probability integral method in the mining area surrounding Yungang Mine.

Name of Coal Mine	Subsidence Coefficient (q)	Horizontal Movement Coefficient (b)	Tangent of Major Influence Angle ($\tan \beta$)	Propagation Angle of Extraction (θ_0)	Inflection Point Offset (S_0)
Datong	0.5	0.3	1.6	$90^\circ - 0.8\alpha$	0.18 H
Sitaigou	0.55	0.25	1.5	$90^\circ - 0.8\alpha$	0.2 H

For the CT3401 working face, backfill mining with gangue is employed. According to relevant research and engineering practices, the subsidence coefficient for backfill mining based on the theory of equivalent mining height is approximately 5% to 10% higher than that for top coal caving with the same mining height [48]. At the same time, referring to Figure 6a, the subsidence coefficient for backfill mining with filling ratios of 80% and 85% after full mining can be calculated as 0.65 using Equation (1). The tangent of the major influence angle is appropriately reduced compared to caving mining with the same mining height. The horizontal movement coefficient and the propagation angle of extraction remain similar to those of caving mining with the same mining height. As depicted in Figure 4, the inflection point is approximately 10 m away from the mining boundary of the working face. Considering the mining depth of the coal seam as 100 m, the inflection point offset is equal to 0.1 H. Based on the predicted parameters of the probability integral method in the surrounding mining area of Yungang Mine, the predicted parameters for surface movement and deformation in the CT3401 working face of Yungang Mine during backfill mining are presented in Table 7.

Table 7. Prediction parameters of the probability integral method for backfill mining in Yungang mine.

Subsidence Coefficient (q)	Horizontal Movement Coefficient (b)	Tangent of Major Influence Angle ($\tan \beta$)	Propagation Angle of Extraction (θ_0)	Inflection Point Offset (S_0)
0.65	0.3	1.5	$90^\circ - 0.8\alpha$	0.1 H

4.3. Design of the Scheme and Analysis of the Results

The five schemes have different filling ratios of 65%, 70%, 75%, 80%, and 85%, corresponding to equivalent mining heights of 0.7 m, 0.6 m, 0.5 m, 0.4 m, and 0.3 m, respectively. A mining subsidence prediction and analysis system based on the principle of the probabil-

ity integral method was utilized to predict the mining subsidence of these five schemes and calculate their surface movement and deformation values. Due to space limitations, a contour map of surface subsidence with only a filling ratio of 85% was plotted, as shown in Figure 9.

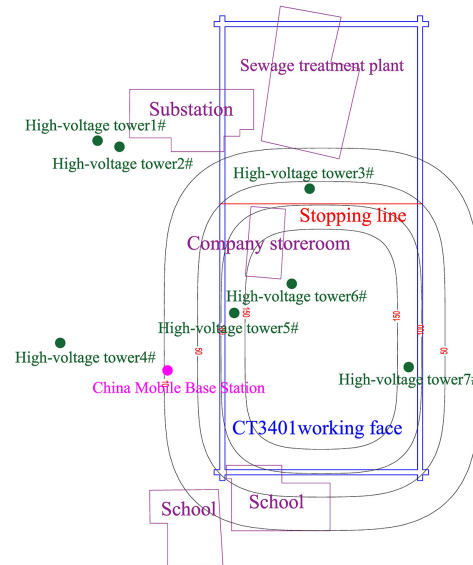


Figure 9. Contour map of surface subsidence with a filling ratio of 85%.

Based on the contour map of surface movement and deformation, the extreme values of movement and deformation for surface buildings and structures were determined for each scheme through statistical analysis, as shown in Table 8. As the curvature deformation in each scheme is negligible, they all fall within the acceptable range of the protection index, and no further statistical analysis was conducted.

Table 8. Extreme values of movement and deformation for surface buildings and structures in each scheme.

Filling Ratio (%)	Maximum Subsidence (mm)	Tilt (mm/m)	Horizontal Migration (mm)	Horizontal Deformation (mm/m)
85	188	2.9	48	1.3
80	252	3.9	72	1.8
75	313	4.8	95	1.9
70	382	5.9	115	2.6
65	439	6.7	138	3.0

Table 4 shows that as the filling ratio increases, the extreme values of movement and deformation for surface buildings and structures decrease continuously. When the filling ratio increases from 65% to 80%, the maximum subsidence value for buildings and structures decreases from 439 mm to 252 mm. The extreme values of tilt decrease from 6.7 mm/m to 3.9 mm/m, and the extreme values of horizontal deformation decrease from 3.0 mm/m to 1.8 mm/m. However, although the extreme values of tilt decrease, they still exceed the protection index. When the filling ratio reaches 85%, the maximum subsidence value for buildings and structures is 188 mm, the extreme value of tilt is 2.9 mm/m, and the extreme value of horizontal deformation is 1.3 mm/m. These values comply with the protection index for surface buildings and structures in the mining area. As the filling ratio continues to increase, it can reduce damage to buildings, but it also leads to higher filling costs, greater technical requirements for filling, and increased economic investments. Based on comprehensive analysis, a filling ratio of 85% is considered the optimal surface subsidence control scheme for backfill mining.

5. Conclusions

- (1) A simulation was conducted to analyze the variation characteristics of maximum surface subsidence with advancing distance for both the toppling and backfill mining methods, with filling ratios of 20%, 40%, 60%, and 80%. It was observed that when the filling ratio is not less than 60%, surface movement and deformation exhibit a continuous and gradual trend, and there is no occurrence of fracture in the hard roof. Practical experience has demonstrated that backfill mining is highly effective in controlling surface movement and deformation during shallow coal seam mining with a hard roof.
- (2) Numerical and physical simulation methods were employed to investigate the characteristics of surface movement and deformation in toppling and backfill mining. It was demonstrated that the surface movement and deformation characteristics in the backfill mining of shallow coal seams with a high filling ratio and a hard roof generally follow the typical surface subsidence patterns observed in fully exploited horizontal coal seams. The prediction model using the probability integral method proved effective in accurately forecasting surface subsidence.
- (3) A prediction method for surface subsidence in backfill mining was proposed. Taking Yungang Mine as an example, five schemes with filling ratios of 65%, 70%, 75%, 80%, and 85% were designed. Finally, considering factors such as the level of damage to surface structures, filling costs, and filling technology, a filling ratio of 85% was determined as the optimal subsidence control scheme.

Author Contributions: Conceptualization, W.H. and H.L.; data curation, W.H. and G.G.; formal analysis, W.H.; funding acquisition, H.L.; investigation, W.H. and Y.W.; methodology, W.H. and H.L.; project administration, G.G.; resources, G.G.; software, G.G.; supervision, G.G. and Y.Y.; visualization, W.H. and Y.W.; writing—original draft, W.H. and H.L.; writing—review and editing, W.H., G.G. and H.L. All authors have read and agreed to the published version of the manuscript.

Funding: This work was funded by the Fundamental Research Funds for the Central Universities (2023ZDPY03).

Institutional Review Board Statement: Not applicable.

Informed Consent Statement: Not applicable.

Data Availability Statement: The data used to support the findings of this study are available from the corresponding author.

Conflicts of Interest: The authors declare no conflict of interest.

References

1. Sheorey, P.R.; Loui, J.P.; Singh, K.B.; Singh, S.K. Ground subsidence observations and a modified influence function method for complete subsidence prediction. *Int. J. Rock Mech. Min. Sci.* **2000**, *37*, 801–818. [[CrossRef](#)]
2. Zhou, J.; Chen, L.; Fu, Z.; Xie, K. Study on Geological Hazards and Countermeasures in Fushun Mining Area. *Appl. Mech. Mater.* **2011**, *71–78*, 4839–4843. [[CrossRef](#)]
3. Vušović, N.; Vlahović, M.; Kržanović, D. Stochastic method for prediction of subsidence due to the underground coal mining integrated with GIS, a case study in Serbia. *Environ. Earth Sci.* **2021**, *80*, 1–29. [[CrossRef](#)]
4. Khanal, M.; Hodgkinson, J.H. Subsidence prediction versus observation in Australia: A short comment. *Environ. Impact Assess. Rev.* **2021**, *86*, 106479. [[CrossRef](#)]
5. Smoliński, A.; Malashkevych, D.; Petlovanyi, M.; Rysbekov, K.; Lozynskyi, V.; Sai, K. Research into Impact of Leaving Waste Rocks in the Mined-Out Space on the Geomechanical State of the Rock Mass Surrounding the Longwall Face. *Energies* **2022**, *15*, 9522. [[CrossRef](#)]
6. Cao, Z.; Xu, P.; Li, Z.; Zhang, M.; Zhao, Y.; Shen, W. Joint Bearing Mechanism of Coal Pillar and Backfilling Body in Roadway Backfilling Mining Technology. *Comput. Mater. Contin.* **2018**, *54*, 137–159.
7. Zhang, J.; Zhou, N.; Huang, Y.; Zhang, Q. Impact law of the bulk ratio of backfilling body to overlying strata movement in fully mechanized backfilling mining. *J. Min. Sci.* **2011**, *47*, 73–84. [[CrossRef](#)]
8. Dai, H.; Yan, Y.; Liu, C.; Zhu, Y.; Bai, Z. Technology of subsidence control by coordinated full-area mining of thick coal seam and application in mining under villages. *J. China Coal Soc.* **2023**. [[CrossRef](#)]

9. Zhang, J.X.; Deng, X.J.; Zhao, X.; Ju, F.; Li, B. Effective control and performance measurement of solid waste backfill in coal mining. *Int. J. Min. Reclam. Environ.* **2017**, *31*, 91–104. [[CrossRef](#)]
10. Guo, G.; Li, H.; Zha, J.; Liu, W.; Hu, Q.; Wang, F.; Chen, C.; Zhang, P.; Zhang, H.; Zhang, Q. Research status and countermeasures of coordinated development of coal mining and cultivated land protection in the plain coal-cropland overlapped areas. *Coal Sci. Technol.* **2023**, *51*, 416–426.
11. Ambrožič, T.; Turk, G. Prediction of subsidence due to underground mining by artificial neural networks. *Comput. Geosci.* **2003**, *29*, 627–637. [[CrossRef](#)]
12. Asadi, A.; Shahriar, K.; Goshtasbi, K.; Najm, K. Development of a new mathematical model for prediction of surface subsidence due to inclined coal-seam mining. *J. South. Afr. Inst. Min. Metall.* **2005**, *105*, 15–20.
13. Unlu, T.; Akcin, H.; Yilmaz, O. An integrated approach for the prediction of subsidence for coal mining basins. *Eng. Geol.* **2013**, *166*, 186–203. [[CrossRef](#)]
14. Sasaoka, T.; Takamoto, H.; Shimada, H.; Oya, J.; Hamanaka, A.; Matsui, K. Surface subsidence due to underground mining operation under weak geological condition in Indonesia. *J. Rock Mech. Geotech. Eng.* **2015**, *7*, 337–344. [[CrossRef](#)]
15. Xuan, D.; Xu, J. Grout injection into bed separation to control surface subsidence during longwall mining under villages: Case study of Liudian coal mine, China. *Nat. Hazards* **2014**, *73*, 883–906. [[CrossRef](#)]
16. Chen, S.; Yin, D.; Cao, F.; Liu, Y.; Ren, K. An overview of integrated surface subsidence-reducing technology in mining areas of China. *Nat. Hazards* **2016**, *81*, 1129–1145. [[CrossRef](#)]
17. Cui, X.; Zhao, Y.; Wang, G.; Zhang, B.; Li, C. Calculation of Residual Surface Subsidence above Abandoned Longwall Coal Mining. *Sustainability* **2020**, *12*, 1528. [[CrossRef](#)]
18. He, J.; Dou, L.; Mu, Z.; Cao, A.; Gong, S. Numerical simulation study on hard-thick roof inducing rock burst in coal mine. *J. Cent. South Univ.* **2016**, *23*, 2314–2320. [[CrossRef](#)]
19. Yang, D.; Zhang, Y.; Chen, Z. Analysis on catastrophe theory during first weighting sliding instability and support crushing of main roof with large mining height in shallow coal seam. *Appl. Sci.* **2020**, *10*, 5408. [[CrossRef](#)]
20. Zheng, K.; Liu, Y.; Zhang, T.; Zhu, J. Mining-induced stress control by advanced hydraulic fracking under a thick hard roof for top coal caving method: A case study in the shendong mining area, China. *Minerals* **2021**, *11*, 1405. [[CrossRef](#)]
21. Chen, D.; Sun, C.; Wang, L. Collapse behavior and control of hard roofs in steeply inclined coal seams. *Bull. Eng. Geol. Environ.* **2021**, *80*, 1489–1505. [[CrossRef](#)]
22. Junker, M.; Witthaus, H. Progress in the research and application of coal mining with stowing. *Int. J. Min. Sci. Technol.* **2013**, *23*, 7–12. [[CrossRef](#)]
23. Gupta, A.K.; Paul, B. A review on utilisation of coal mine overburden dump waste as underground mine filling material: A sustainable approach of mining. *Int. J. Min. Miner. Eng.* **2015**, *6*, 172–186. [[CrossRef](#)]
24. Huang, P.; Spearing, A.J.S.; Feng, J.; Jessu, K.V.; Guo, S. Effects of solid backfilling on overburden strata movement in shallow depth longwall coal mines in West China. *J. Geophys. Eng.* **2018**, *15*, 2194–2208. [[CrossRef](#)]
25. Fu, Z.; Zhou, L.; Yu, K.; Li, W.; Chen, H. Field Measurement and Study on Overburden Fracture and Surface Subsidence Law of Solid Filling Mining under Buildings. *Shock. Vib.* **2021**, *2021*, 5265333. [[CrossRef](#)]
26. Jiang, N.; Wang, C.; Pan, H.; Yin, D.; Ma, J. Modeling study on the influence of the strip filling mining sequence on mining-induced failure. *Energy Sci. Eng.* **2020**, *8*, 2239–2255. [[CrossRef](#)]
27. Zhang, J.; Yan, H.; Zhang, Q.; Li, B.; Zhang, S. Disaster-causing mechanism of extremely thick igneous rock induced by mining and prevention method by backfill mining. *Eur. J. Environ. Civ. Eng.* **2020**, *24*, 307–320. [[CrossRef](#)]
28. Lyashenko, V.; Khomenko, O.; Golik, V.; Topolnij, F.; Helevera, O. Substantiation of environmental and resource-saving technologies for void filling under underground ore mining. *Technol. Audit. Prod. Reserves* **2020**, *2*, 52. [[CrossRef](#)]
29. Jiřina, T.; Jan, Š. Reduction of surface subsidence risk by fly ash exploitation as filling material in deep mining areas. *Nat. Hazards* **2010**, *53*, 251–258. [[CrossRef](#)]
30. Bai, E.; Guo, W.; Tan, Y.; Yang, D. The analysis and application of granular backfill material to reduce surface subsidence in China's northwest coal mining area. *PLoS ONE* **2018**, *13*, e0201112. [[CrossRef](#)]
31. Liu, S.; Bai, J.; Wang, G.; Wang, X.; Wu, B. A method of backfill mining crossing the interchange bridge and application of a ground subsidence prediction model. *Minerals* **2021**, *11*, 945. [[CrossRef](#)]
32. Sun, Q.; Zhang, J.; Qi, W.; Li, M. Backfill mining alternatives and strategies for mitigating shallow coal mining hazards in the western mining area of China. *Q. J. Eng. Geol. Hydrogeol.* **2020**, *53*, 217–226. [[CrossRef](#)]
33. Vu, T.T.; Do, S.A. Determination of the rock mass displacement zone by numerical modeling method when exploiting the longwall at the Nui Beo Coal Mine, Vietnam. *Min. Miner. Depos.* **2023**, *17*, 59–66. [[CrossRef](#)]
34. Hu, B.; Zhang, Q.; Li, S.; Yu, H.; Wang, X.; Wang, H. Application of numerical simulation methods in solving complex mining engineering problems in dingxi mine, China. *Minerals* **2022**, *12*, 123. [[CrossRef](#)]
35. Babanouri, N.; Beyromvand, H.; Dehghani, H. Evaluation of different methods of pillar recovery in coal mining by numerical simulation: A case study. *Environ. Earth Sci.* **2023**, *82*, 110. [[CrossRef](#)]
36. Sun, W.; Zhang, Q.; Luan, Y.; Zhang, X. A study of surface subsidence and coal pillar safety for strip mining in a deep mine. *Environ. Earth Sci.* **2018**, *77*, 627. [[CrossRef](#)]
37. Wesołowski, M.; Mielińska, R.; Jendruś, R.; Popczyk, M. Influence Analysis of Mine Flooding from the Environmental Standpoint: Surface Protection. *Pol. J. Environ. Stud.* **2018**, *27*, 905–915. [[CrossRef](#)]

38. Rajwa, S.; Janoszek, T.; Świątek, J.; Walentek, A.; Bałaga, D. Numerical Simulation of the Impact of Unmined Longwall Panel on the Working Stability of a Longwall Using UDEC 2D—A Case Study. *Energies* **2022**, *15*, 1803. [[CrossRef](#)]
39. Wu, F.; Chen, B.; Zou, Q.; Zhai, C.; Liu, W.; Chen, J.; Ni, G. Range estimation of horizontal stress of deep rock based on Mohr–Coulomb criterion. *Results Phys.* **2019**, *12*, 2107–2111. [[CrossRef](#)]
40. Shen, J.; Priest, S.D.; Karakus, M. Determination of Mohr–Coulomb shear strength parameters from generalized Hoek–Brown criterion for slope stability analysis. *Rock Mech. Rock Eng.* **2012**, *45*, 123–129. [[CrossRef](#)]
41. Singh, A.; Rao, K.S.; Ayothiraman, R. Study on Mohr–Coulomb-based three-dimensional strength criteria and its application in the stability analysis of vertical borehole. *Arab. J. Geosci.* **2019**, *12*, 578. [[CrossRef](#)]
42. Ai, Y.; Zhao, J.; Wang, H.; He, W. Prediction of surface collapse for Sitaigou Coal Mine in Datong. *Environ. Sci.* **1988**, *13*, 87–90.
43. Hou, Z.; Zhang, Y. Movement law of coal mining subsidence surface ground in Datong Mining Area. *Coal Sci. Technol.* **2004**, *2*, 50–53.
44. Deng, K.; Tan, Z.; Jiang, Y. *Deformation Monitoring and Settlement Engineering*; China University of Mining and Technology Press: Xuzhou, China, 2014.
45. Xu, J. *Law and Application of Evolution of Mining-Induced Fractures in Rock Strata*; China University of Mining and Technology Press: Xuzhou, China, 2016.
46. China Administration of Safety Supervision; China Administration of Coal Mine Safety Supervision; China Energy Administration. *Code for Coal Pillar Retention and Coal Mining under Building, Water Body, Railway and Main Shafts*; China Coal Industry Press: Beijing, China, 2014.
47. Miao, X.; Zhang, J.; Guo, G. Study on waste-filling method and technology in fully-mechanized coal mining. *J. China Coal Soc.* **2010**, *35*, 1–6.
48. Guo, G.-L.; Zhu, X.-J.; Zha, J.-F.; Wang, Q. Subsidence prediction method based on equivalent mining height theory for solid backfilling mining. *Trans. Nonferrous Met. Soc. China* **2014**, *24*, 3302–3308. [[CrossRef](#)]

Disclaimer/Publisher’s Note: The statements, opinions and data contained in all publications are solely those of the individual author(s) and contributor(s) and not of MDPI and/or the editor(s). MDPI and/or the editor(s) disclaim responsibility for any injury to people or property resulting from any ideas, methods, instructions or products referred to in the content.